SOIL, 10, 795–812, 2024
https://doi.org/10.5194/soil-10-795-2024

SOIL Open Access EGU

Investigating the complementarity of thermal and physical soil organic carbon fractions

Amicie A. Delahaie[1], Lauric Cécillon[1], Marija Stojanova[1], Samuel Abiven[1], Pierre Arbelet[2], Dominique Arrouays[3], François Baudin[4], Antonio Bispo[3], Line Boulonne[3], Claire Chenu[5], Jussi Heinonsalo[6], Claudy Jolivet[3], Kristiina Karhu[6], Manuel Martin[3], Lorenza Pacini[1,2], Christopher Poeplau[7], Céline Ratié[3], Pierre Roudier[8], Nicolas P. A. Saby[3], Florence Savignac[4], and Pierre Barré[1]

[1]Laboratoire de Géologie, École Normale Supérieure, CNRS, PSL University, IPSL, Paris, France
[2]Greenback (commercial name: Genesis), Paris, France
[3]INRAE, Info&Sols, 45075, Orléans, France
[4]UMR ISTeP 7193, Sorbonne Université, CNRS, Paris, France
[5]UMR ECOSYS, INRAE, AgroParisTech, Université Paris Saclay, 91123 Palaiseau, France
[6]Department of Forest Sciences, Faculty of Agriculture and Forestry, University of Helsinki, Helsinki, Finland
[7]Thünen Institute of Climate-Smart Agriculture, Braunschweig, Germany
[8]Manaaki Whenua – Landcare Research, Te Papaioea / Palmerston North, Aotearoa / New Zealand

Correspondence: Amicie A. Delahaie (amicie.delahaie@ens.fr)

Received: 22 January 2024 – Discussion started: 2 February 2024
Revised: 8 June 2024 – Accepted: 1 July 2024 – Published: 12 November 2024

Abstract. Partitioning soil organic carbon (SOC) in fractions with different biogeochemical stability is useful to better understand and predict SOC dynamics and provide information related to soil health. Multiple SOC partition schemes exist, but few of them can be implemented on large sample sets and therefore be considered relevant options for soil monitoring. The well-established particulate organic carbon (POC) vs. mineral-associated organic carbon (MAOC) physical fractionation scheme is one of them. Introduced more recently, Rock-Eval® thermal analysis coupled with the $\text{PARTY}_{\text{SOC}}$ machine learning model can also fractionate SOC into active (C_a) and stable SOC (C_s). A debate is emerging as to which of these methods should be recommended for soil monitoring. To investigate the complementarity or redundancy of these two fractionation schemes, we compared the quantity and environmental drivers of SOC fractions obtained on an unprecedented dataset from mainland France. About 2000 topsoil samples were recovered all over the country, presenting contrasting land cover and pedoclimatic characteristics, and analysed. We found that the environmental drivers of the fractions were clearly different, the more stable MAOC and C_s fractions being mainly driven by soil characteristics, whereas land cover and climate had a greater influence on more labile POC and C_a fractions. The stable and labile SOC fractions provided by the two methods strongly differed in quantity ($\text{MAOC}/C_s = 1.88 \pm 0.46$ and $\text{POC}/C_a = 0.36 \pm 0.17$; $n = 843$) and drivers, suggesting that they correspond to fractions with different biogeochemical stability. We argue that, at this stage, both methods can be seen as complementary and potentially relevant for soil monitoring. As future developments, we recommend comparing how they relate to indicators of soil health such as nutrient availability or soil structural stability and how their measurements can improve the accuracy of SOC dynamics models.

Published by Copernicus Publications on behalf of the European Geosciences Union.

1 Introduction

Evaluating the biogeochemical stability of soil organic carbon (SOC) is crucial for predicting future SOC stock changes and assessing soil health. SOC biogeochemical stability depends on many interacting factors such as soil organic matter (SOM) molecular composition and interactions with the mineral matrix (von Lützow et al., 2006; Schmidt et al., 2011). For a given soil, SOC represents a continuum of mean residence times (MRTs) ranging from days to millennia (Balesdent, 1996). However, this continuum cannot be measured directly and then used efficiently for evaluating SOC biogeochemical stability. For this reason, many studies have proposed SOC fractionation schemes to distinguish fractions with contrasting residence times, enabling a practical assessment of SOC biogeochemical stability (Poeplau et al., 2018). Nevertheless, many of these fractionation methods are expensive and time-consuming, making their use on large datasets almost impossible.

Recently, Lavallee et al. (2020) proposed a drastic simplification of the SOC biogeochemical stability continuum by dividing SOC into two fractions of contrasted stability: particulate organic carbon (POC) and mineral-associated organic carbon (MAOC) fractions, following on early work by Cambardella and Elliott (1992). This physical fractionation scheme is relatively quick and can be implemented on hundreds of samples (Lugato et al., 2021), and recent studies have underlined the potential interest of such a dualistic view of the SOC persistence continuum (Cécillon, 2021; Angst et al., 2023; Lugato et al., 2021).

Less popular than physical fractionation, thermal fractionation has also been proposed as an efficient method to evaluate SOC quality (Plante et al., 2009). In particular, Rock-Eval® thermal analysis has been the subject of growing interest in recent years in assessing SOC biogeochemical stability (Saenger et al., 2013; Barré et al., 2016; Sebag et al., 2016; Soucémarianadin et al., 2018). This method is relatively fast and can be used to analyse a series of thousands of samples (Delahaie et al., 2023). Moreover, Cécillon et al. (2018, 2021) developed a machine learning model, $\text{PARTY}_{\text{SOC}}$, which uses Rock-Eval® thermal analyses results as input variables to estimate the proportion of SOC that is stable at a centennial scale and, by difference, the proportion of SOC that is active at this timescale. Kanari et al. (2022) showed that the fractions determined by $\text{PARTY}_{\text{SOC}}$ match the "stable" and "active" fractions of the AMG model (Clivot et al., 2019), improving its simulations of SOC stock evolutions in croplands. As a result, Rock-Eval® thermal analysis associated with $\text{PARTY}_{\text{SOC}}$ allows SOC to be partitioned into a more labile fraction (C_a), with an MRT ranging from 20 to 40 years, and a stable fraction (C_s), which can be considered inert at a centennial timescale.

The POC/MAOC physical fractionation and the C_a/C_s thermal fractionation are therefore two methods that can potentially be used to split SOC into fractions with contrasted biogeochemical stability and be implemented on large sample sets. With the growing interest in monitoring programmes of soil health and the need for better initialization methods able to improve the accuracy of SOC dynamics models, it is necessary to assess the extent to which these two fractionation approaches are complementary or redundant.

Our hypotheses were that as they do not target the same SOC pools (Balesdent, 1996; Poeplau et al., 2018; Kanari et al., 2022), POC and C_a as well as MAOC and C_s fractions may represent different quantities and have different environmental drivers (soil characteristics, land cover, and climate variables) and can therefore be considered complementary. To test our hypotheses, we used an unprecedented dataset comprising ca. 2000 Rock-Eval® thermal analyses and ca. 1000 POC/MAOC physical fractionation data from the analysis of topsoil (0–30 cm) samples that are part of the French soil monitoring network (RMQS).

2 Material and methods

2.1 RMQS soil samples

The soil samples used in this article are part of the French "Réseau de mesures de la qualité des sols" (RMQS) network and were previously described in Gogé et al. (2012) and Delahaie et al. (2023). A complete description of this monitoring network is available in Jolivet et al. (2006, 2022). Briefly, French mainland soils are monitored every 15 years following a 16 km × 16 km regular square grid, resulting in 2170 sites. When possible, the sampling site is set at the centre of the cell; alternatively, another site is selected if needed within a 1 km radius from the centre of the cell. At each sampling site, 25 topsoil samples (0 to 30 cm or tilled layer depth, whichever depth is smaller) are taken from a 20 m × 20 m area using a spiral auger and then mixed, resulting in a composite sample of 5 to 10 kg.

The composite samples are then placed in trays and air-dried at 30 °C for 8 to 10 d and quartered according to NF ISO 11464, resulting in a subsample of ca. 650 g. They are then hand-crushed and sieved at 2 mm, and an aliquot is ground under 250 µm by a Cyclotec 1093 (FOSS) (Gogé et al., 2012). The remains of the samples are stored in plastic buckets.

A total of 2037 samples from the first sampling campaign (2000–2009) out of 2170 were recovered and analysed by Rock-Eval® thermal analysis in Delahaie et al. (2023).

2.2 Soil and environmental data associated with each RMQS site and topsoil sample

2.2.1 Soil data

Physical and chemical analyses were carried out on composite soil samples at the Laboratoire d'Analyse des Sols (INRAE, Arras, France). The inorganic carbon content (C_{inorg}) was derived from the total carbonate content, in grams per

kilogram of sample (volumetric method, NF EN ISO 10693), and calculated as C_{inorg} = total carbonate × 0.12; the total carbon content, in grams per kilogram of sample, was determined by elemental analysis using dry combustion on non-decarbonated soil; the organic carbon content was derived from the elemental analysis (TOCea), in grams per kilogram of sample, and calculated as total carbon content minus inorganic carbon content, i.e. TOCea − C_{inorg} (NF ISO 10694; "NF" standing for French standard); the total nitrogen, in grams per kilogram of sample, was determined by dry combustion (NF ISO 13878); the particle size distribution was measured without decarbonation, in grams per kilogram of sample (Robinson pipette and underwater sieving, method validated in relation to standard NF X31-107); pH was measured in a suspension of soil diluted with water (dilution 1 : 5, NF ISO 10390); the exchangeable calcium content, in centimoles per kilogram of sample, was measured by cobaltihexammine chloride extraction (NF X31-130); the exchangeable magnesium content, in centimoles per kilogram of sample, was measured by cobaltihexammine chloride extraction (NF X31-130); the exchangeable potassium content, in centimoles per kilogram of sample, was measured by cobaltihexammine chloride extraction (NF X31-130); and the free iron oxides, in grams per 100 g, were measured with the Tamm method in the dark (amorphous oxides) and the Mehra–Jackson method (crystalline oxides) (INRA standard/NF ISO 22036).

2.2.2 Climate data

We allocated the climatic data corresponding to the SAFRAN 8 km × 8 km grid cell to each sampling site based on where the cell was located (https://publitheque.meteo.fr/okapi/accueil/okapiWebPubli/index.jsp, last access: 31 March 2022). The daily data were averaged over the 1969–1999 period (i.e. the 30-year common period before the first sampling campaign started in 2000) in order to compute the mean annual temperature (MAT) and mean annual precipitation (MAP) for each site.

2.2.3 Land cover data

Land cover data were recorded during sampling. Four main categories of land cover were considered for this study: "croplands", "forests", "grasslands", and "vineyards and orchards". A few samples were collected in "wastelands", "urban parks", and "sites with little human disturbance". Considering the very small number of samples, "wastelands" (ca. 10) and "gardens" ($n = 3$) were not included in this study. The number of samples from environments with little human disturbance (ca. 30) could potentially be considered sufficient for statistical treatment; however, these samples represent a very heterogeneous set (10 miscellaneous subclasses, such as peatlands, alpine grasslands, water edge vegetation, heath, and dry siliceous meadows). Thus, those sites were also discarded.

2.3 Thermal SOC fractionation

2.3.1 Rock-Eval® thermal analyses

In total, 2037 samples were analysed by Rock-Eval® thermal analysis (Disnar et al., 2003; Baudin et al., 2015). For each sample, ca. 60 mg of finely ground matter (< 250 µm) was placed in a special high-temperature-resistant stainless-steel pod, allowing the transport gas to pass through, and then placed inside a Rock-Eval® 6 (RE6) Turbo device (Vinci Technologies). There, it underwent a first phase of pyrolysis under an inert atmosphere (N_2) from ambient temperature to 650 °C (3 min isotherm at 200 °C and then a temperature ramp of 30 °C min^{-1}) and a second phase of oxidation under the laboratory atmosphere purged from water and CO_2, from 300 to 850 °C (1 min isotherm at 300 °C and then a temperature ramp of 20 °C min^{-1}). During the pyrolysis phase, hydrocarbon effluents were monitored by a flame ionization detector, and CO and CO_2 were monitored by infrared detectors. During the oxidation phase, CO and CO_2 were monitored by infrared detectors. The resulting thermograms were processed using the Geoworks software (Geoworks V1.6R2, Vinci Technologies, 2021).

The organic carbon yield was defined as the ratio of the total organic carbon amount measured by Rock-Eval® thermal analysis (TOCre6, calculated from thermogram area integration) over the total organic carbon amount measured by elemental analysis (TOCea). We chose to apply a quality criterion on this yield: further study was only conducted on samples with an organic carbon yield ranging from 0.7 to 1.3. This range was set to identify the acceptable yields ensuring the quality of the Rock-Eval® analysis as well as the identity of the sample. Of the 2037 samples analysed by Rock-Eval® thermal analysis, 1891 presented an organic carbon yield ranging from 0.7 to 1.3 (Delahaie et al., 2023). We also removed 12 samples with TOCea > 120 g kg^{-1} to avoid organic soils (Eggleston et al., 2006), resulting in a dataset of 1879 samples.

2.3.2 The $PARTY_{SOC}$ fractionation

The $PARTY_{SOC}$ model (Cécillon et al., 2018, 2021) is a machine learning model using the results of the Rock-Eval® thermal analysis of mineral topsoils as entry variables. This model, trained on data from long-term agronomic experiments, uses 18 Rock-Eval® parameters – associated with either thermal stability or chemical composition – as input variables and determines the proportion of the centennially persistent organic carbon pool in a mineral topsoil sample. By taking into account both the chemical recalcitrance and the stabilization brought by the organic matter–mineral interactions, this model recognizes different aspects of the biogeochemical stability, not limited to the chemistry

alone. The stable SOC proportion is now calculated routinely by the Geoworks software (Geoworks V1.6R2, Vinci Technologies, 2021) using the model $\text{PARTY}_{\text{SOC}}$ v2.0EU published in Cécillon et al. (2021). For each site, we multiply the proportion of stable C by the TOCea to calculate the conceptual C_s pool (g C kg^{-1} sample); the conceptual active pool C_a (g C kg^{-1} sample) is obtained by difference, i.e. $C_a = \text{TOCea} - C_s$.

2.4 Physical SOC fractionation

The physical SOC fractionation, i.e. particle size fractionation, was conducted by the SADEF laboratory (Aspach-Le-Bas, France) on a subset of the RMQS (997 sites) following a protocol based on the norm NF X 31-516, itself based on Balesdent et al. (1991, 1998). The dispersion was carried out with a solution of sodium hexametaphosphate at a concentration of $5\,\text{g L}^{-1}$. A quantity of 50 g of soil sieved at 2 mm was stirred into 180 mL of hexametaphosphate solution with 10 glass beads of 5 mm diameter and underwent rotary agitation for 16 h at 20 °C at 45 rpm in a 250 mL flask. The fractions were then sieved by hand at 0.2 mm with rotative movements, and sprays of demineralized water were used to complete the sieving process. The matter remaining on the sieve was transferred in a capsule, dried, and crushed. The suspension containing the fine particles (< 0.2 mm) and rinsing water was collected for further sieving to 0.05 mm. The same principle was then applied for the sieving at 0.05 mm, but it was conducted on three or four successive fractions of the suspension to avoid clogging the sieve. The liquid fraction containing the particles below 0.05 mm was recovered in a 1 L crystallizer and dried. The drying of the fractions was carried out in a ventilated oven at 105 °C.

This fractionation process thus resulted in three fractions: the mineral-associated organic matter (MAOM) fraction corresponds to the 0–50 µm fraction, the fine particulate organic matter fraction corresponds to the 50–200 µm fraction, and the coarse particulate organic matter fraction corresponds to the 200–2000 µm fraction. The carbon contained in the MAOM fraction constitutes the MAOC, while the carbon contained in both the fine particulate organic matter (POM) and coarse POM constitutes the POC.

After drying, all the dry matter in each fraction was recovered. Each fraction was introduced into a corundum bowl and ground with corundum balls (Retch PM400 planetary ball mill) at 400 rpm for 5 min to ensure the final matter is ground at < 250 µm and homogenized.

Carbon and nitrogen measurements were carried out on a Flash 2000 elemental analyser for soils without carbonates (determined by acid test) following the norms NF ISO 10694 and NF ISO 13878, respectively. For carbonated soils, only nitrogen was measured on the Flash 2000 elemental analyser (Dumas method NF ISO 13878). Organic carbon was analysed by chemical oxidation (NF ISO 14235). The total organic carbon retrieved after physical fractionation is denoted TOCfr, and the organic carbon yield for this fractionation was defined as the ratio of TOCfr over TOCea.

The C yield was on average 93.4 % for the 997 samples. For the same reasons as above, we also introduced a quality criterion on this yield, identical to the one for the Rock-Eval® results (0.7 to 1.3). Following this rule, 33 samples were removed from the dataset. Then, four samples with TOCea > $120\,\text{g kg}^{-1}$ were also removed to avoid organic soils (Eggleston et al., 2006), resulting in a final dataset comprising 960 fractionation results. The samples removed showed no particular pedoclimatic characteristics (Fig. A2).

As the physical and thermal fractionations were not conducted on all the samples, there are samples for which data of only one method were available. The intersection of the physical fractionation dataset and thermal fractionation dataset consists of 843 samples and is thereafter designated as the "intersection dataset".

2.5 Statistical analysis

2.5.1 The determination of drivers of the POC, MAOC, C_a, C_s, and TOCea quantities

In this study, we tested the influence of different environmental variables on the C_s, C_a, MAOC, and POC content using random forest (RF) regression models based on the method used by Georgiou et al. (2022). One advantage of random forest models is that they can cope with non-normally distributed and correlated variables (Breiman, 2001). The considered environmental drivers were related to soil characteristics (particle size distribution, pH, inorganic carbon content, exchangeable cations contents (calcium, magnesium, potassium), amorphous and crystalline iron oxyhydroxides contents), climate (mean annual precipitation, mean annual temperature), and land cover. The relative importance of each of these features as estimated by the random forest model allowed us to evaluate the main drivers of the quantity of each fraction.

The modelling pipeline was divided into two steps. The first preprocessing step used one-hot encoding (creating one Boolean column per class for any categorical variable; one-hot encoding was chosen in order to handle categorical variables without establishing any artificial ranking between them), while all the numeric variables were standardized by removing their mean and dividing them by their variances. In the second step, a bootstrapped random forest regressor was used to calibrate the actual model. Grid search and cross-validation were used to choose the model's hyper-parameters (Table A1), using cross-validated R^2 (determination coefficient) as a performance metric. These hyper-parameters define the structure and construction of the forest's trees, and as such they are crucial and must be chosen wisely to ensure that the model does not overfit or underfit the training data.

After the model was calibrated, the importance of the environmental predictors was calculated using two different

methods: the mean decrease in impurity (MDI) and the permutation importance (PI) score (Louppe, 2014). Both methods gave a measurement of the importance of the environmental variables selected in the model. The MDI aims at selecting the predictors that, on average, produce trees with the purest nodes and leaves. In this case, purity refers to the similarity of the samples contained in a single leaf. The MDI is calculated using the training set, and it is the default decision metric used in constructing scikit-learn's random forests. However, the MDI has a known tendency to lower the importance of the low-cardinality variables and possibly has a bias towards highly correlated variables (Louppe et al., 2013). The PI score measures the impact of each individual predictor by randomly permuting it and then calculating the increase in prediction error as opposed to using the non-permuted predictor. By construction, PI can be calculated on both the training and the test set. Its main advantage over the MDI is that it shows no bias towards high-cardinality predictors. Highly correlated variables can be detected using PI as their permutation will have little to no impact on the model's prediction accuracy.

In order to analyse the variable importance results, the environmental variables were grouped into three broad categories: "land cover", "pedology" (particle size distribution, pH, inorganic carbon content, exchangeable calcium content, exchangeable magnesium content, exchangeable potassium content, amorphous, and crystalline iron oxyhydroxides contents), and "climate" (mean annual temperature and mean annual precipitation). These groupings were used to guide visual analysis of the variable importance plots generated for the C_s, C_a, MAOC, and POC models.

The random forest modelling (and associated metrics) was done in Python as implemented in the scikit-learn v1.3.0 library (Pedregosa et al., 2011), while the least-squares linear regression used the SciPy v1.10.1 library (Virtanen et al., 2020).

2.5.2 Assessments of the effect of land cover on fractions

To assess the effect of land cover on the different fractions, we performed pairwise comparisons of medians using non-parametric Kruskal–Wallis tests ($p < 0.05$) followed by Wilcoxon tests, with $p < 0.05$ for each pair. The correction of p values within the framework of the multiple comparisons was done using the Holm–Bonferroni method. Correlations between parameters were calculated using the Spearman method.

The data processing and statistical analysis were carried out using R software (V4.1.2; R Core Team, 2021): the corrplot (Wei and Simko, 2021), car (Fox and Weisberg, 2019), ggplot2 (Wickham, 2016), ggpubr (Kassambara, 2023a), factoextra (Kassambara and Mundt, 2020), plot3D (Soetaert, 2021), and rstatix (Kassambara, 2023b) packages were added.

3 Results

3.1 POC vs. C_a and MAOC vs. C_s: fractions and conceptual pools in different quantities

Figure 1 shows the quantities of C_s plotted against MAOC and the quantities of C_a plotted against POC, comparing the more stable and more labile fractions two by two for each fractionation scheme for the intersection dataset (samples having been subjected to both thermal and physical fractionation schemes). Regarding the more stable fractions (Fig. 1a), the MAOC content was much higher than the C_s content (on average $19.13\,g\,kg^{-1}$ of sample vs. $10.06\,g\,kg^{-1}$ of sample for the 843 samples of the intersection dataset). The average ratio of $MAOC/C_s$ for the samples of the intersection dataset was 1.88 ± 0.46. For the more labile fractions (Fig. 1b), the POC content was much lower than the C_a content (on average $5.32\,g\,kg^{-1}$ of sample vs. $14.40\,g\,kg^{-1}$ of sample for the 843 samples of the intersection dataset). The average ratio of POC/C_a for the samples of the intersection dataset was 0.36 ± 0.17. These results are very close to those obtained when excluding the samples with TOCea values outside the $PARTY_{SOC}$ model learning range (5–41.5 $g\,kg^{-1}$ of sample; see Fig. A1). The correlations between C_s and MAOC on the one side (0.90) and between C_a and POC on the other side (0.87) are both very significant. In comparison, the correlation coefficients between C_s, MAOC, and C_a and POC on the one hand and TOC on the other hand are 0.91, 0.96, 0.98, and 0.86, respectively.

3.2 Differences in SOC fractions' proportions under different land cover

Figure 2 shows C_a and POC as a proportion of TOC for the four considered land cover types. As $C_a + C_s$ and POC + MAOC were equal to TOC, the analysis on C_s or MAOC proportions would have given the same information. Figure 2 shows that the proportion of C_a of the TOC followed the order vineyards and orchards < croplands < grasslands < forests (and similarly for POC). The mean values of the proportion of C_a were 0.48, 0.60, 0.63, and 0.35 in croplands, grasslands, forests, and vineyards, respectively. It also shows that POC as a proportion of TOC was significantly smaller in croplands compared to forests, grasslands, and vineyards and orchards, but the median value of POC in croplands was close to the median value in grasslands (0.13 in croplands, 0.17 in grasslands, 0.27 in forests, and 0.19 in vineyards and orchards). As with the median values, the mean values showed a similar difference between croplands (0.15 ± 0.05) and grasslands (0.19 ± 0.07), with forests displaying a higher value (0.28 ± 0.09). While the C_a fraction generally represents a high proportion of TOC (up to 0.75 in forests; proportion of $C_a > 0.5$ in 1277 out of 1879 samples), POC most often represented only a minority of TOC (proportion of POC > 0.5 in 17 out of 960 samples).

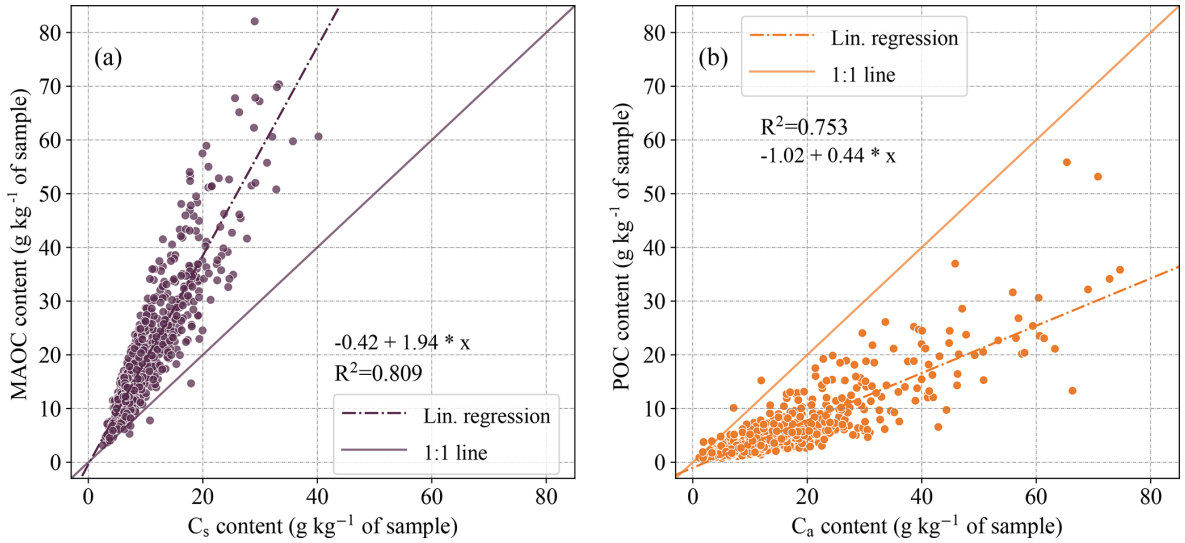

Figure 1. Comparison of the quantities of the more stable and more labile fractions for the physical and thermal SOC fractionation schemes, with their correlation coefficient R^2 and linear regression. Panel **(a)** shows the quantities of MAOC plotted against C_s. Panel **(b)** shows the quantities of POC plotted against C_a. The dataset is the intersection dataset, i.e. samples for which thermal and physical data are available ($n = 843$).

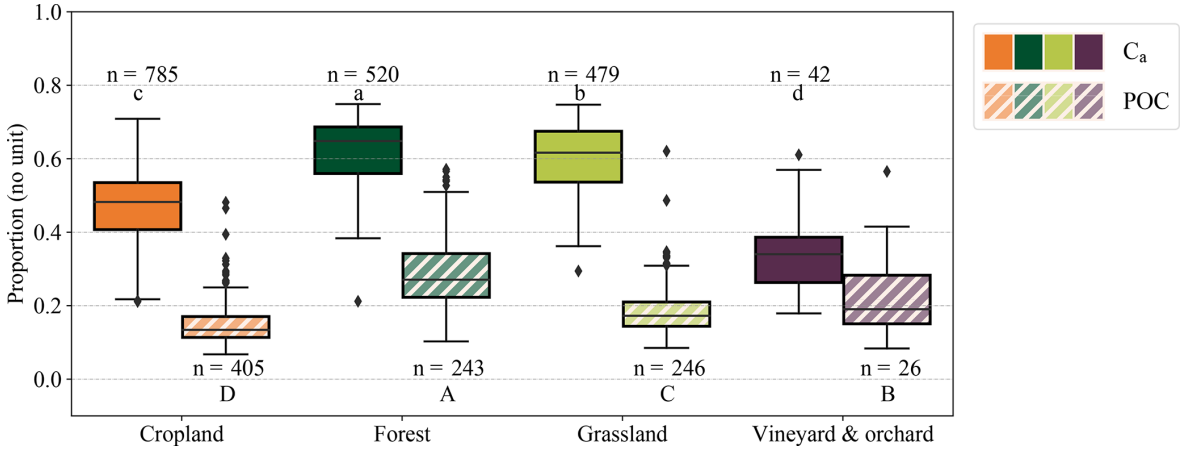

Figure 2. Proportion of the C_a and POC fractions depending on the land cover. The black line in each box is the median, the lower and upper edges of the black rectangle are the respective first ($Q1$) and third ($Q3$) quartiles, and the lower and upper whiskers are the maximum between the minimum value or the first quartile minus 1.5 times the interquartile range (max[min; $Q_1 - 1.5 \times (Q_3 - Q_1)$]) and the minimum between the maximum or the third quartile plus 1.5 times the interquartile range (min[max; $Q_3 + 1.5 \times (Q_3 - Q_1)$]), respectively. Different letters indicate significant differences in the distribution of the values for the land cover according to a Kruskal–Wallis test ($p < 0.05$) and a pairwise Wilcoxon rank sum test ($p < 0.05$); lowercase letters are used for C_a and uppercase for POC.

Additionally, different ratios (MAOC/C_s and POC/C_a) are given in Fig. A3. Croplands and grasslands exhibited a similar and small POC/C_a ratio, while forests and vineyards and orchards show a higher POC/C_a ratio. Conversely, the MAOC/C_s ratio is very small in the vineyards and orchards and the highest in grasslands, with a significant difference between croplands and grasslands.

3.3 Drivers of the different SOC fraction quantities

The random forest models fitted for the four different SOC fractions and conceptual pools aimed at elucidating the relative importance of the soil and environmental variables. Their explanatory capacity was evaluated based on the R^2 values obtained for each fraction. The random forest models' R^2 scores on the test set were 61 % for C_s, 53 % for MAOC, 57 % for C_a, 36 % for POC, and 58 % for TOCea (Fig. A3). The R^2 values obtained through cross-validation of the train-

ing set were higher but close (Table A1), except for the POC which has a strongly higher training set score. Overall, the models' performance was satisfactory and allowed their variable importance to be analysed.

Figure 3 shows the importance of the different categories of environmental variables on the quantities of POC, C_a, MAOC, and C_s, evaluated using two different methods. The results with both the MDI and PI showed a higher importance of the pedological features and a smaller importance of climate and land cover in the more stable fractions (C_s and MAOC). Conversely, the more labile fractions (C_a and POC) showed a higher importance of land cover and, to a lesser extent, climate, compared to C_s and MAOC. C_a tended to show a slightly stronger influence of climate and weaker influence of land cover, while POC rather showed the opposite. Among the more stable fractions, climate and land cover tended to have a slightly higher importance for MAOC than for C_s. The results for the TOCea showed a mixture of drivers in between stable and labile fractions.

The results for the Spearman correlation coefficients between all environmental variables and fractions' quantities are given in Table A2 in the Appendix. Soil variables favouring organic matter–mineral interactions (clay, metallic oxides, cation-exchange capacity (CEC), exchangeable calcium) were positively correlated with fractions. Overall, these correlations were stronger for the C_s and MAOC fractions. On average, iron oxyhydroxides and exchangeable cations are the most important factors influencing the size of the fractions (Fig. 3). Carbonates and pH little influenced the size of the fractions and texture had a minor role but for C_s. Regarding climate variables, MAT had a higher influence than MAP except for C_s fractions.

4 Discussion

4.1 A strong influence of land cover on the more labile SOC fractions

This study, based on an unprecedented number of measurements ($n = 960$ for POC/MAOC and $n = 1879$ for C_a/C_s), shows the high influence of land cover on the relative quantity of SOC labile and stable fractions and conceptual pools (Fig. 2).

The higher proportion of POC in forest than in grassland and cropland soils (0.13, 0.17, and 0.27 in croplands, grasslands, and forests, respectively) was also observed in Lugato et al. (2021), who used results from 352 physical fractionations obtained using a fractionation protocol similar to ours on samples from the LUCAS soil monitoring network. It was also observed by Hansen et al. (2024) in a global dataset combining physical fractions obtained with different protocols. Other studies showed similar results for POC, but comparisons are less straightforward as the physical fractionation protocols used are significantly different from those used in our study. For instance, some studies used the protocol of Zimmermann et al. (2007), where the sorting size for POC is $> 63\,\mu m$ (compared with $> 50\,\mu m$ in our protocol) and part of POC is also recovered after the disruption of sand-sized aggregates. When combining free POC and occluded POC (which corresponds to what is called POC in our study), Poeplau and Don (2013) found proportions of POC of 0.15 in croplands, 0.21 in grasslands, and 0.27 in forests in a variety of sites across Europe, which is very close to the values observed here for French soils. The value of 0.13 for the proportion of POC in croplands is also close to the 0.15 value used in Angers et al. (2011) to estimate the proportion of POC from TOC. Chen et al. (2019) gathered data from multiple previous studies to derive POC proportion values of 0.15 for croplands, 0.31 for grasslands, and 0.34 for forests.

Regarding the C_a conceptual pool, we found a higher proportion of C_a in forest than in grassland and cropland soils (0.48, 0.62, and 0.65 in croplands, grasslands, and forests, respectively). This was also observed in previous works, but the body of literature available for discussion is much more limited than for physical fractionation. We can note that the median value of C_a for croplands is close to the mean value (0.48 vs 0.42) obtained by Kanari et al. (2022) on nine long-term field experiments in mainland France. Moreover, the proportion of C_a is set to 0.60 in the AMG model for grasslands (Clivot et al., 2019) in its default parameterization, which is also in line with the C_a proportions observed for grassland sites of the RMQS (0.62 on average). The difference is bigger regarding croplands as the default parameterization for C_a is set to 0.35, while the value found for the RMQS is 0.48. This may be explained by the fact that the AMG model was developed on long-term experimental sites that have been cropped for several decades, whereas French agricultural soils have probably on average undergone more changes in vegetation cover. The higher C_a value in RMQS cropland soils could thus be due to a difference in land cover history in French cropland soils compared to cropland sites of long-term experiments. Indeed, the land cover history is likely to be reflected in the results: the croplands with lower C_s proportions could likely be former grasslands or forests recently converted to agriculture. On the other hand, grasslands or forests with high C_s proportions were probably former croplands before being afforested or converted to grasslands. The results for forests shall be taken with caution, as the $PARTY_{SOC}$ model has not been trained on forests' soils. However, the results are realistic and consistent. It is also worth mentioning that by its nature, the random forest model used in $PARTY_{SOC}$ cannot extrapolate outside its training values. While 85 % of the RMQS samples fall inside the training values, it is possible that some unusual C_a or C_s values come from "outsider" samples.

The similar proportions of POC in vineyards and orchards and grasslands were less expected as C inputs and contents are reduced in vineyards and orchards (grass cover was very sparse in vineyards and orchards at the time of the sampling). This may be explained by differences in the com-

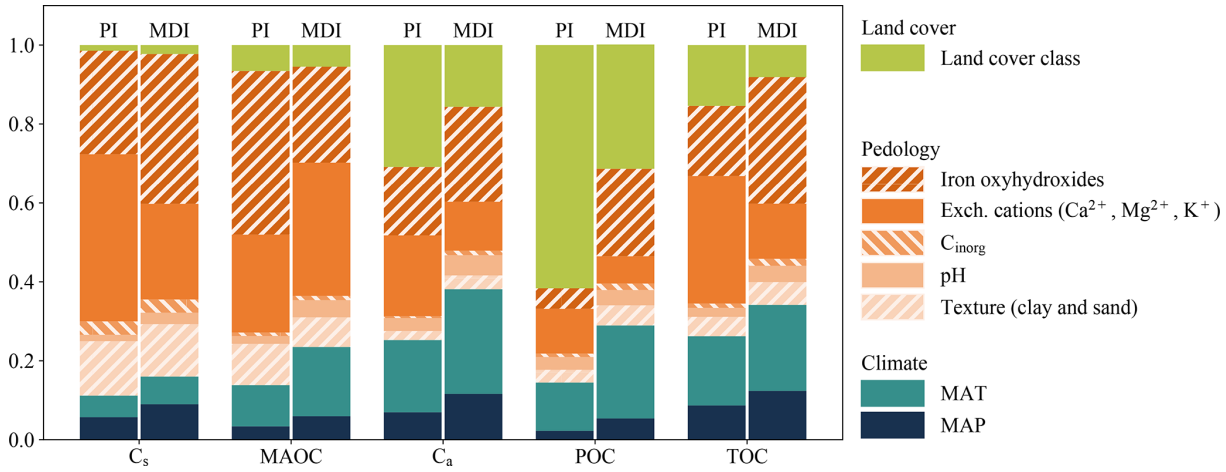

Figure 3. Importance of the different categories of soil and environmental variables (climate, pedology, and land cover) for the four fractions C_s, MAOC, C_a, and POC and with TOCea as a comparison (in $g\,C\,kg^{-1}$ sample), assessed using the MDI and PI.

position of the particulate organic matter for the different land cover types, as the particulate organic matter groups together particles that can be biochemically quite heterogeneous (Schrumpf et al., 2013; Soucémarianadin et al., 2019). In our study, the POC fraction in vineyards and orchards topsoils might be much more biogeochemically stable than the same fraction in cropland and grassland topsoils because of the presence of more lignified woody debris and pyrogenic C derived from the combustion of vine shoots. An extreme example of soil with high proportion of POC and C_s can be found at the Versailles long-term bare fallow site where topsoils have a proportion of C_s close to 1 and a POC proportion around 0.30, constituted essentially of charcoal (Chassé et al., 2021). Our results therefore suggest that POC/MAOC fractionation gives an erroneous view of biogeochemical stability for vineyards and orchards, which have the same POC proportion as grassland but are very C depleted (9.5 vs. 24 $g\,C\,kg^{-1}$). The biochemical nature of the fractions is unaccounted for in our study as these data are not available, but it is probably an important driver for POC quantities. The fact that such an important driver is not taken into account may explain the poorer performance of the model for POC compared to the other fractions (36 % vs. 55 %–60 % for the other fractions).

Regarding the mean values of all the fractions and conceptual pools in the four major land cover types (Table A3), it is interesting to note that there is a 45 % loss of SOC between grasslands and croplands on average (50 % between forests and croplands). Specifically, this loss between grasslands and croplands (and between forests and croplands) is 61 % (and 74 %) for POC, 55 % (and 61 %) for C_a, 41 % (and 35 %) for MAOC, and 27 % (and 30 %) for C_s. It highlights a loss ranking as follows: POC > C_a > MAOC > C_s; the bulk SOC has intermediate loss values, which is consistent with the results from Sanderman et al. (2021), showing a 30 % loss of bulk SOC between grasslands and croplands.

4.2 SOC fractions with different quantities, drivers, and biogeochemical stabilities

The significant differences between the C_s and MAOC quantities on the one side and C_a and POC quantities on the other side (Fig. 1) show that they do not correspond to the same fractions. This result was expected due to the definition of the four fractions, but it is evidenced for the first time on a large dataset. Indeed, previous studies using isotopic measurements observed that the mean residence times for MAOC ranged from decades to centuries (Anderson and Paul, 1984; Balesdent et al., 1987; Balesdent, 1996; von Lützow et al., 2007; Kleber et al., 2015). By definition, C_s corresponds to the conceptual pool of centennially stable SOC (Cécillon et al., 2018, 2021). This implies that MAOC also encompasses a certain amount of relatively labile SOC and therefore explains its larger quantity compared to C_s. Potentially, this could partly be related to the fractionation method itself, in which only size fractionation is employed to separate fractions, so that the MAOC fraction might also contain a certain amount of fine POC or soluble compounds (Lavallee et al., 2020; Cotrufo et al., 2023). Conversely, the C_a fraction which corresponds to the SOC fraction with a mean residence time of 20–40 years (Kanari et al., 2022) is larger than the POC fractions dominated by SOC with a generally shorter MRT (Balesdent, 1996; von Lützow et al., 2007).

This ranking in terms of the MRT, C_s > MAOC > C_a > POC, is also in line with the different environmental drivers explaining the quantities of these four fractions, whatever the selected method (the MDI or PI) (Fig. 3). Indeed, we observed that the importance of land cover is much higher for POC and C_a than it is for C_s and MAOC, whereas pedological variables are much more important for C_s and MAOC

fractions. The importance of land cover for SOC with a lower MRT has already been documented in several studies. For instance, Poeplau and Don (2013) observed that POC fractions are very sensitive to land cover in topsoils, and Balesdent et al. (2018) showed that land cover is a major driver of the incorporation of "young" C in topsoils, indicating a smaller portion of SOC with a low MRT in croplands on average compared to grassland and forest topsoils. The fact that SOC with a higher MRT is mostly driven by soil variables and that SOC with a lower MRT is mainly explained by land cover and climate was also evidenced by Mathieu et al. (2015) using ^{14}C in 122 profiles of mineral soil across the world. They observed that the age of topsoil organic carbon, which is on average less biogeochemically stable than deep SOC, was primarily affected by climate and land cover, whereas the age of deep soil carbon was affected more by soil type and soil characteristics such as clay content and mineralogy. With a slightly different physical fractionation – POC, humus OC, and resistant OC – and different, numerous variables, Viscarra-Rossel et al. (2019) showed that POC was influenced by climate (mostly MAT) but little by vegetation; in contrast, the resistant OC showed less influence by climate and vegetation compared to the POC and humus OC, and above all, it highlighted the difference between drivers at the global scale (Australia) vs. regional scale (seven subdivisions). The little influence of land cover on the stable fractions was somehow expected as most of French soils have undergone a series of land cover changes during the last millennia during which the stable fraction formed. Regarding the bulk SOC, our results are in line with those of Edlinger et al. (2023), who used a similar methodology on a smaller dataset to investigate the drivers of SOC. While their features were not strictly identical to ours (no iron oxyhydroxides for instance, but more climatic features), the main categories that stand out as drivers of the SOC are pedology (mostly exchangeable calcium) and climate, which is what we observed.

Among pedological variables, iron oxyhydroxides (mostly crystalline oxides) and exchangeable cations (mainly calcium cations) were the factors with the greatest influence on the size of the most stable C_s and MAOC fractions. The strong influence of exchangeable cations and oxides on MAOC has also been recently documented in a study involving 16 agricultural sites in the United States (King et al., 2023). The influence of iron oxides and hydroxides on SOC biogeochemical stability is a well-known fact (Kögel-Knabner et al., 2008), although it was pointed out that crystalline oxides were less efficient at providing bonding sites for SOM. The importance of exchangeable cations, notably calcium, on SOC biogeochemical stability was previously documented (Rowley et al., 2018, 2021). Indeed, calcium cations can strengthen the interactions between 2 : 1 clay minerals and SOM, both negatively charged, or enable the formation of co-precipitates with SOM.

Overall, our study confirms results from recent studies conducted at regional and global scales showing that physical fractions have different drivers (King et al., 2023; Hansen et al., 2024) and strongly supports the idea that it is relevant and informative to consider SOC fractions (either physical or thermal) instead of TOC alone. However, it is difficult to compare our results directly with those of these recent studies. Indeed, the data processing strategies are different and the explanatory variables considered are not the same. Notably, we observed that land cover and soil variables such as exchangeable calcium and iron oxides were explanatory variables of primary importance in explaining the quantities of POC and MAOC, respectively. These variables were not considered explanatory variables in the path analyses developed by Hansen et al. (2024), which likely explains the low explained variations provided by these path analyses. Conversely, we did not consider net primary production (NPP) an explanatory variable, which was found to be a significant driver of MAOC quantities by Hansen et al. (2024). We therefore consider that new data that will probably arrive in the next few years will enable us to refine the drivers of physical and thermal fractions at different spatial scales.

4.3 Which fractionation method should be used to assess SOC biogeochemical stability in soil monitoring networks?

Several recent high-level political initiatives have highlighted the importance of soil health for food security and climate change mitigation and adaptation. These include, for instance, the UNFCCC "Koronivia joint work on agriculture" action, the "4 per 1000" initiative (http://www.4p1000.org, last access: 28 November 2023, Rumpel et al., 2020), and the new soil monitoring law proposed by the EU. These initiatives emphasize the importance of SOC by highlighting the C sequestration potential of soils or by stressing the strong influence of SOC on soil health. This general political context is favourable to the development and support of soil monitoring networks. In these networks, SOC content is always measured. While these data are important, information on SOC biogeochemical stability would be particularly useful. Indeed, most soil functions related to SOM, such as nitrogen mineralization, actually depend on its decay (Janzen, 2006), and assessing biogeochemical stability is also of primary importance to simulate SOC stock evolution (Luo et al., 2016). In this context, the development of indicators of SOC biogeochemical stability that can be implemented on large sample sets is of particular relevance.

Both physical and thermal fractionation methods are good candidates for this. Indeed, they both split SOC into two fractions or conceptual pools of different biogeochemical stability using protocols that can be applied to large sample sets. Each has its advantages and drawbacks regarding its large-scale implementation for soil monitoring. The thermal method is faster (1 h per sample); highly reproducible (Pacini

et al., 2023); and, at least in France, less costly than the physical method (EUR < 50 per sample vs. EUR > 100 per sample in commercial laboratories), but it only provides virtual fractions. POC/MAOC fractionation, on the other hand, requires much time but no expensive equipment and is already used worldwide. Moreover some studies have proposed to predict POC/MAOC fractions using a machine learning model to make the method faster (Cotrufo et al., 2019; Lugato et al., 2021). However, a recent study showed that the results of such prediction methods can be questionable and even misleading (Begill et al., 2023).

In this context, the question arises as to what method should be used to determine biogeochemical stability in soil monitoring networks. Our study, based on an unprecedented sample set, reveals that the POC vs. C_a and MAOC vs. C_s fractions are significantly different in size and do not have exactly the same environmental drivers, meaning that they are not biogeochemically equivalent. This suggests that the two fractionation methods provide, at least partly, different information and could be, at that stage, seen as complementary. Furthermore, they can also be used to answer different questions: for example, physical fractionation methods can be used, in combination with isotopic measurements (e.g. ^{13}C), to study transformation and stabilization processes of organic matter in soils (Cotrufo et al., 2015). Moreover, it is probably premature to assess the relevance of the two protocols at this stage, as interesting data will be provided by the monitoring networks over the next few years. For instance, with new SOC stock measurement campaigns, it will be possible to have measurements of SOC stock evolution, allowing the proper evaluation of model SOC stock projections at network scales (Le Noë et al., 2023). In addition, several indicators of soil functions are to be measured at large scale for soil health assessment. All these new data will enable us to assess the extent to which the information on SOC biogeochemical stability provided by fractionation results can be used to improve the accuracy of SOC stock evolution simulations and to gain a better understanding of soil functioning. Such upcoming studies are likely to bring new key elements to the emerging question of the redundancy or complementarity of physical and thermal fractionation schemes. New analyses could also be performed by Rock-Eval® analysis on soil samples before and after the specific removal of POM by flotation. This could help disentangle the composition of the C_a and C_s pools in terms of POC and MAOC.

5 Conclusion

This study allowed us to compare the POC/MAOC physical fractionation and thermal fractionation on an unprecedented number of samples with an interesting diversity with respect to pedological characteristics, climatic characteristics, and land cover. We showed that both the stable (C_s and MAOC) and labile (C_a and POC) fractions strongly differ in quantities. While the environmental drivers were close for the two stable fractions (and the two labile fractions), with a predominance of the soil characteristics (and the climate and land cover), they still presented differences, suggesting that C_s and MAOC (and C_a and POC) correspond to different fractions with different biogeochemical stability. This means that both fractionation techniques display different and thus complementary information. Future work will enable us to discuss the relevance of one technique rather than the other on a case-by-case basis, depending on the soil properties studied.

Appendix A

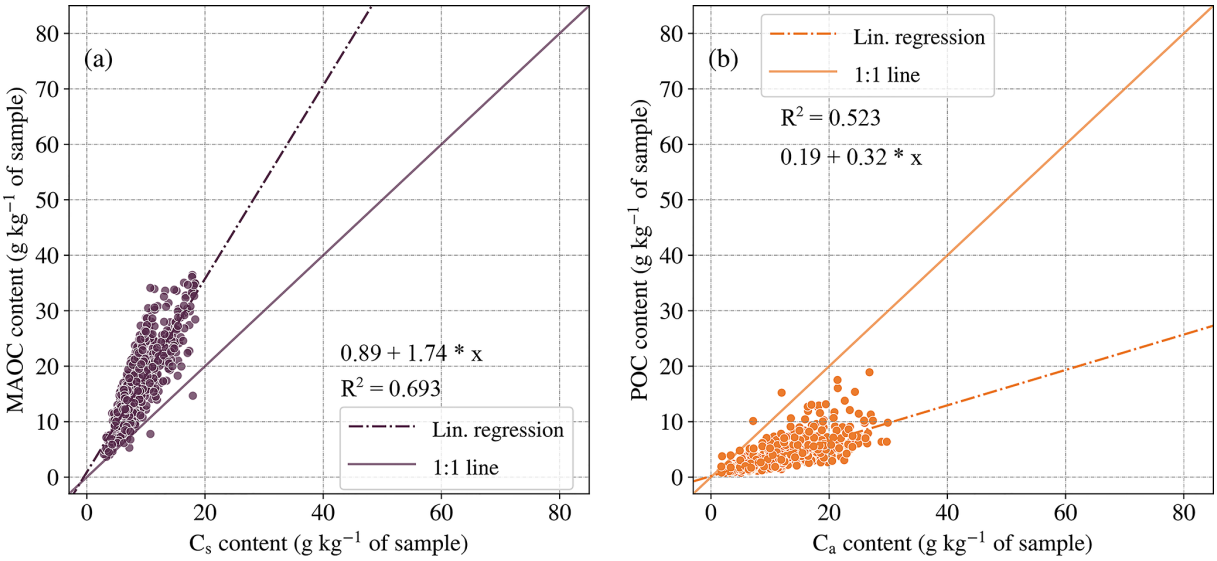

Figure A1. Comparison of the quantities of the more stable and more labile fractions for the physical and thermal SOC fractionation schemes, with their correlation coefficient R^2 and linear regression, limited to samples with a TOCea value comprised between 5 and 41.5 g kg^{-1} of sample (included). Panel **(a)** shows the quantities of MAOC plotted against C_s. Panel **(b)** shows the quantities of POC plotted against C_a. The dataset is the intersection dataset, i.e. samples for which thermal and physical data are available, with the same TOCea limitations as in the $PARTY_{SOC}$ model training ($n = 735$).

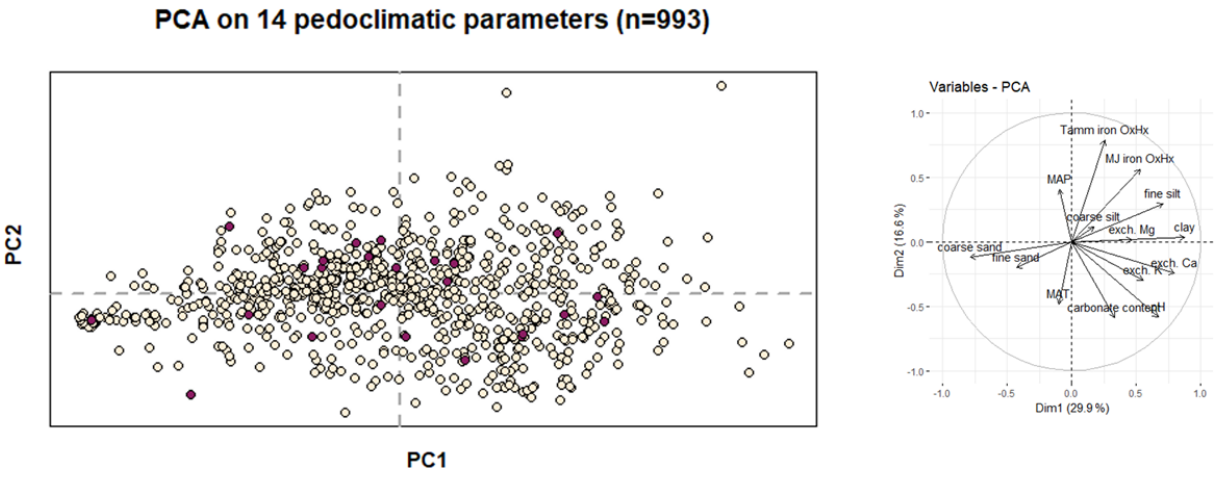

Figure A2. Score of the 993 samples on axes 1 and 2 of the principal component analysis (PCA) on 14 pedoclimatic parameters: clay, fine silt, coarse silt, fine sand, and coarse sand contents; pH in water; carbonate content; mean annual temperature and mean annual precipitation; Tamm and Mehra–Jackson iron oxyhydroxide contents; and exchangeable calcium, magnesium, and potassium ions. Samples with an organic carbon yield between 0.7 and 1.3 are plotted in light yellow, whereas samples with an organic carbon yield < 0.7 or > 1.3 are plotted in dark red.

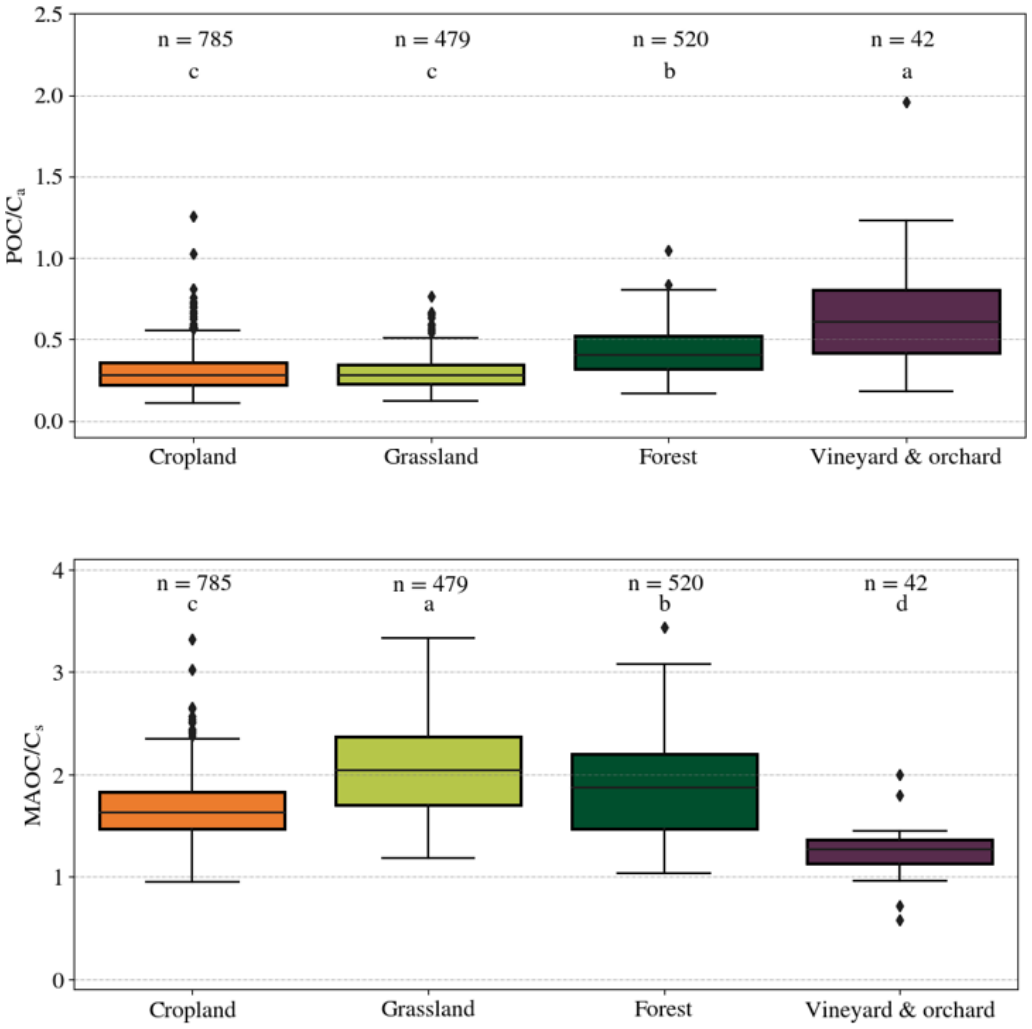

Figure A3. Ratios of the fractions for the four major land covers. The black line in each box is the median, the lower and upper edges of the black rectangle are the respective first ($Q1$) and third ($Q3$) quartiles, and the lower and upper whiskers are the maximum between the minimum value or the first quartile minus 1.5 times the interquartile range (max[min; $Q1 - 1.5 \times (Q3 - Q1)$]) and the minimum between the maximum or the third quartile plus 1.5 times the interquartile range (min[max; $Q3 + 1.5 \times (Q3 - Q1)$]), respectively. Different letters indicate significant differences in the distribution of the values for the land covers according to a Kruskal–Wallis test ($p < 0.05$) and a pairwise Wilcoxon rank sum test ($p < 0.05$).

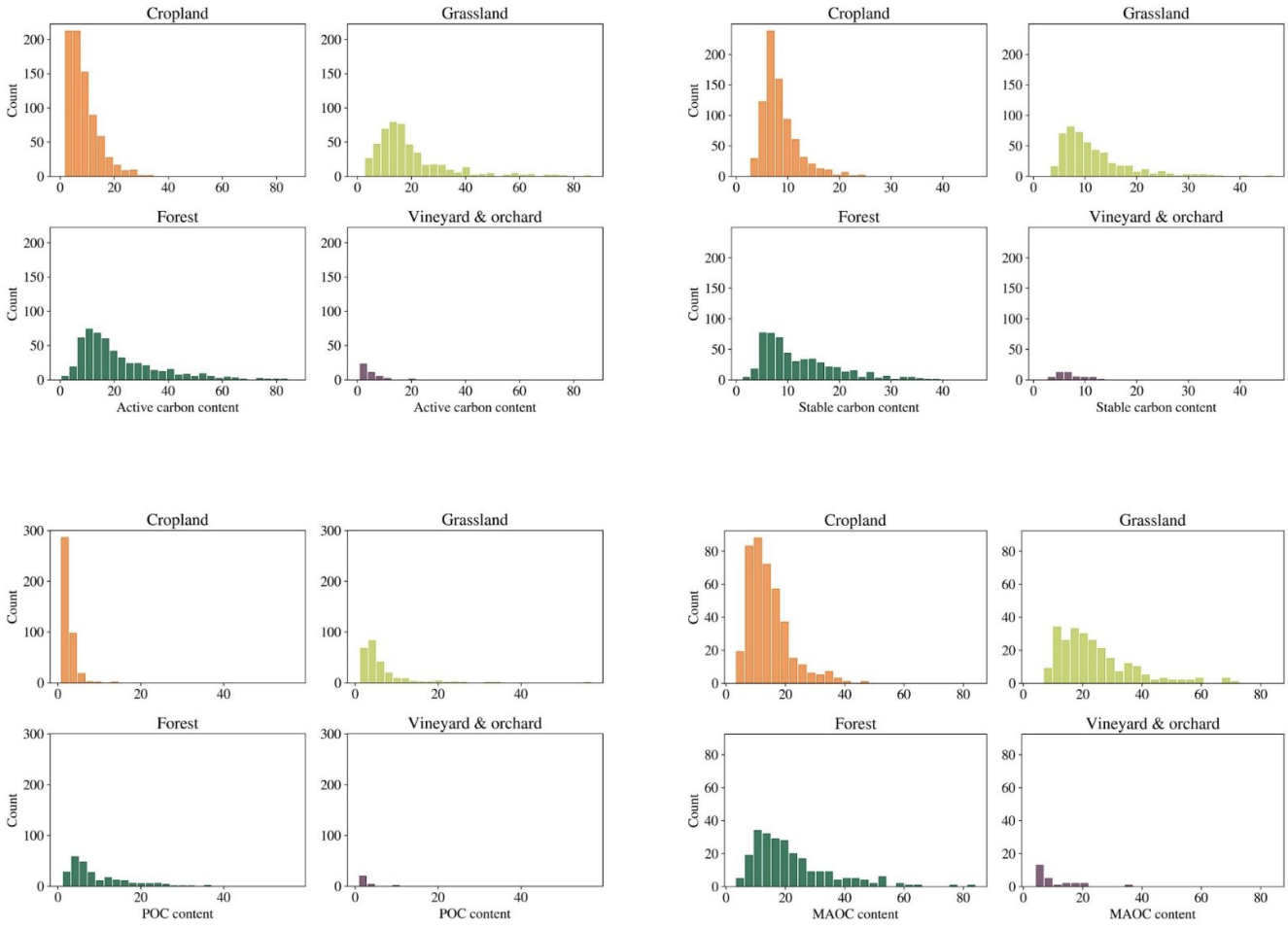

Figure A4. Histograms of the fractions and conceptual pools contents in $g\,kg^{-1}$ of soil, depending on the four major land covers.

Table A1. Hyper-parameters used by the random forest model for TOC and the four fractions of SOC.

	C_a quantity	C_s quantity	TOC	MAOC quantity	POC quantity
RF training accuracy	0.639	0.707	0.667	0.690	0.668
RF testing accuracy	0.574	0.616	0.583	0.525	0.352
Number of estimators	200	600	400	600	200
Maximum number of features per tree	0.33	0.33	0.33	0.33	0.33
Maximum tree depths	4	4	4	4	4
Minimum number of samples per node	5	3	5	5	3
Minimum number of samples per leaf	3	3	3	5	3

Table A2. Spearman correlation coefficients of the C_a content, C_s content, C_s proportion, POC content, MAOC content, POC proportion, C_s/MAOC, MAOC − C_s, POC/C_a, and C_a − POC with the following pedoclimatic variables for the RMQS topsoil (0–30 cm) samples: clay, total silt, total sand, TOCea, C/N ratio, mean annual temperature (MAT) averaged over 1969–1999, mean annual precipitation (MAP) averaged over 1969–1999, pH in water, carbonate content (InoC), Tamm iron oxyhydroxides (crystalline), Mehra–Jackson iron oxyhydroxides (amorphous), cation exchange capacity (CEC), exchangeable calcium, exchangeable magnesium, exchangeable potassium, exchangeable aluminium, exchangeable iron, exchangeable sodium, and exchangeable manganese. The analysis was limited to samples meeting the required criterion for Rock-Eval® thermal analysis and/or physical fractionation. The number of samples presenting data for each calculation is indicated. Absolute values ≥ 0.3 are in bold. The asterisks and superscript letters indicate p values: *** between 0 and 0.001, ** between 0.001 and 0.01, * between 0.01 and 0.05, a between 0.05 and 0.1, and $b > 0.1$. The values in italics have non-significant p values.

		C_s content	C_a content	C_s proportion		MAOC content	POC content	POC proportion		C_s/MAOC	MAOC −C_s	POC/C_a	C_a− POC
Clay	$n = 1879$	**0.52** ***	0.23 ***	0.15 ***	$n = 958$	**0.39** ***	0.18 ***	−0.15 ***	$n = 843$	0.17 ***	0.17 ***	*−0.06* *b*	0.22 ***
Total silt	$n = 1879$	*−0.04* *b*	−0.12 ***	0.17 ***	$n = 958$	*−0.04* *b*	−0.18 ***	**−0.37** ***	$n = 843$	*−0.06* *a*	*−0.05* *b*	−0.22 ***	−0.12 ***
Total sand	$n = 1879$	−0.28 ***	*−0.04* *a*	−0.22 ***	$n = 958$	−0.20 ***	*0.03* *b*	**0.36** ***	$n = 843$	*−0.06* *b*	*−0.06* *a*	0.20 ***	*−0.04* *b*
TOCea	$n = 1879$	**0.91** ***	**0.98** ***	**−0.53** ***	$n = 960$	**0.96** ***	**0.86** ***	**0.32** ***	$n = 843$	−0.27 ***	**0.82** ***	*0.01* *b*	**0.90** ***
C/N	$n = 1879$	0.11 ***	0.29 ***	**−0.40** ***	$n = 959$	0.12 ***	**0.39** ***	**0.60** ***	$n = 843$	*−0.03* *b*	0.11 **	**0.30** ***	0.17 ***
MAT 1969–1999	$n = 1879$	**−0.30** ***	**−0.45** ***	**−0.39** ***	$n = 960$	**−0.38** ***	**−0.30** ***	−0.08 *	$n = 843$	**0.33** ***	**−0.41** ***	0.11 **	**−0.40** ***
MAP 1969–1999	$n = 1879$	**0.34** ***	**0.37** ***	−0.27 ***	$n = 960$	**0.37** ***	0.29 ***	0.14 ***	$n = 843$	−0.16 ***	**0.35** ***	*−0.02* *b*	**0.38** ***
pH	$n = 1879$	0.15 ***	−0.20 ***	**0.55** ***	$n = 960$	−0.12 ***	−0.17 ***	−0.21 ***	$n = 843$	**0.43** ***	−0.26 ***	*0.04* *b*	−0.25 ***
InoC	$n = 1879$	0.11 ***	*−0.03* *b*	0.16 ***	$n = 958$	*0.00* *b*	*−0.04* *b*	*−0.05* *b*	$n = 843$	0.14 ***	*−0.04* *b*	*−0.03* *b*	*−0.03* *b*
Tamm iron	$n = 1610$	**0.38** ***	**0.43** ***	−0.25 ***	$n = 823$	**0.51** ***	0.28 ***	−0.09 *	$n = 714$	−0.24 ***	**0.49** ***	−0.16 ***	**0.49** ***
Mehra–Jackson iron	$n = 1609$	**0.49** ***	0.27 ***	0.06 *	$n = 822$	**0.39** ***	0.23 ***	*−0.05* *b*	$n = 713$	0.09 *	0.22 ***	*0.03* *b*	0.25 ***
CEC	$n = 1879$	**0.61** ***	**0.31** ***	0.13 ***	$n = 960$	**0.39** ***	0.27 ***	*−0.05* *b*	$n = 843$	0.21 ***	0.16 ***	*0.02* *b*	0.21 ***
Exch. Ca	$n = 1879$	**0.56** ***	0.25 ***	0.18 ***	$n = 960$	**0.33** ***	0.20 ***	−0.08 *	$n = 843$	0.24 ***	0.10 **	*0.02* *b*	0.15 ***
Exch. Mg	$n = 1879$	0.25 ***	0.15 ***	*0.04* *a*	$n = 960$	0.15 ***	0.15 ***	0.07 *	$n = 843$	0.15 ***	*0.02* *b*	0.07 *	0.07 *
Exch. K	$n = 1879$	0.10 ***	*−0.04* *a*	0.18 ***	$n = 960$	*0.03* *b*	−0.08 *	−0.21 ***	$n = 843$	0.15 ***	*−0.06* *b*	−0.07 *	*−0.05* *b*
Exch. Al	$n = 1879$	0.11 ***	**0.39** ***	**−0.45** ***	$n = 960$	**0.37** ***	**0.33** ***	0.21 ***	$n = 843$	**−0.33** ***	**0.43** ***	*−0.01* *b*	**0.45** ***
Exch. Fe	$n = 1879$	0.26 ***	**0.35** ***	−0.22 ***	$n = 960$	0.28 ***	**0.31** ***	0.17 ***	$n = 843$	−0.10 **	0.25 ***	0.08 *	0.29 ***
Exch. Na	$n = 1879$	*−0.01* *b*	*−0.02* *a*	0.08 ***	$n = 958$	*−0.02* *b*	*0.00* *b*	0.09 **	$n = 843$	*0.04* *b*	*0.01* *b*	*0.04* *b*	*0.02* *b*
Exch. Mn	$n = 1851$	*−0.04* *a*	0.09 ***	−0.18 ***	$n = 947$	*−0.04* *b*	*0.05* *b*	0.12 ***	$n = 832$	−0.15 ***	*−0.00* *b*	*0.04* *b*	*−0.01* *b*

Table A3. Mean values of the different fractions and conceptual pools in g kg^{-1} of soil for the four major land covers.

	TOC	POC	MAOC	C_a	C_s	POC/MAOC	C_a/C_s
Croplands	16.89	2.37	14.20	8.52	8.37	0.17	1.02
Grasslands	30.19	6.04	23.89	18.74	11.45	0.25	1.64
Forests	33.33	9.09	21.76	21.39	11.95	0.42	1.79
Vineyards and orchards	11.47	2.68	10.23	4.40	7.07	0.26	0.62

Code availability. The code for the random forest and the plots is available on Zenodo https://doi.org/10.5281/zenodo.10551240 (Stojanova and Delahaie, 2024).

Data availability. The results of the Rock-Eval® thermal analyses are freely available at https://doi.org/10.57745/KVUTRB (Delahaie et al., 2024). The data on basic soil properties are available at https://doi.org/10.15454/BNCXYB (Saby et al., 2019).

Author contributions. AAD, LC, PB, FB, and CC designed the study. FS and FB produced the Rock-Eval® thermal analyses. DA, AB, LB, CJ, MM, CR, and NPAS provided the detailed pedoclimatic data. AAD processed and interpreted the data with the contribution of all co-authors. MS wrote the random forest algorithm and provided technical support for the use of the code. AAD and PB wrote the manuscript with contributions from all the co-authors.

Competing interests. At least one of the (co-)authors is a member of the editorial board of *SOIL*. The peer-review process was guided by an independent editor, and the authors also have no other competing interests to declare.

Disclaimer. Publisher's note: Copernicus Publications remains neutral with regard to jurisdictional claims made in the text, published maps, institutional affiliations, or any other geographical representation in this paper. While Copernicus Publications makes every effort to include appropriate place names, the final responsibility lies with the authors.

Acknowledgements. The École Normale Supérieure of Paris is greatly acknowledged for the funding of the PhD thesis grant of Amicie Delahaie. Pierre Roudier is funded by the Aotearoa / New Zealand Government to support the objectives of the Global Research Alliance on Agricultural Greenhouse Gases. We thank Sophie Cornu for helping us to recover the RMQS sample collection.

Financial support. This research has been supported by the Agence de l'Environnement et de la Maîtrise de l'Energie (grant no. 2003C0017). The FREACS project was funded by the external call of the EJP Soil (ANR-22-SOIL-0001).

Review statement. This paper was edited by Moritz Laub and reviewed by Katerina Georgiou and one anonymous referee.

References

Anderson, D. W. and Paul, E. A.: Organo-mineral complexes and their study by radiocarbon dating, Soil Sci. Soc. Am. J., 48, 298–301, https://doi.org/10.2136/sssaj1984.03615995004800020014x, 1984.

Angers, D. A., Arrouays, D., Saby, N. P. A., and Walter, C.: Estimating and mapping the carbon saturation deficit of French agricultural topsoils, Soil Use Manage., 27, 448–452, https://doi.org/10.1111/j.1475-2743.2011.00366.x, 2011.

Angst, G., Mueller, K. E., Castellano, M. J., Vogel, C., Wiesmeier, M., and Mueller, C. W.: Unlocking complex soil systems as carbon sinks: multi-pool management as the key, Nat. Commun., 14, 2967, https://doi.org/10.1038/s41467-023-38700-5, 2023.

Balesdent, J.: The significance of organic separates to carbon dynamics and its modelling in some cultivated soils, Eur. J. Soil Sci., 47, 485–493, https://doi.org/10.1111/j.1365-2389.1996.tb01848.x, 1996.

Balesdent, J., Mariotti, A., and Guillet, B.: Natural ^{13}C abundance as a tracer for studies of soil organic matter dynamics, Soil Biol. Biochem., 19, 25–30, https://doi.org/10.1016/0038-0717(87)90120-9, 1987.

Balesdent, J., Pétraud, J. P., and Feller, C.: Effets des ultrasons sur la distribution granulométrique des matières organiques des sols, Science du Sol, 29, 95–106, 1991.

Balesdent, J., Besnard, E., Arrouays, D., and Chenu, C.: The dynamics of carbon in particle-size fractions of soil in a forest-cultivation sequence, Plant Soil, 201, 49–57, https://doi.org/10.1023/A:1004337314970, 1998.

Balesdent, J., Basile-Doelsch, I., Chadoeuf, J., Cornu, S., Derrien, D., Fekiacova, Z., and Hatté, C.: Atmosphere–soil carbon transfer as a function of soil depth, Nature, 559, 599–602, https://doi.org/10.1038/s41586-018-0328-3, 2018.

Barré, P., Plante, A. F., Cécillon, L., Lutfalla, S., Baudin, F., Bernard, S., Christensen, B. T., Eglin, T., Fernandez, J. M., Houot, S., Kätterer, T., Le Guillou, C., Macdonald, A., van Oort, F., and Chenu, C.: The energetic and chemical signatures of persistent soil organic matter, Biogeochemistry, 130, 1–12, https://doi.org/10.1007/s10533-016-0246-0, 2016.

Baudin, F., Disnar, J. R., Aboussou, A., and Savignac, F.: Guidelines for Rock–Eval analysis of recent marine sediments, Org. Geochem., 86, 71–80, https://doi.org/10.1016/j.orggeochem.2015.06.009, 2015.

Begill, N., Don, A., and Poeplau, C.: No detectable upper limit of mineral-associated organic carbon in temperate agricultural soils, Global Change Biol., 29, 4662–4669, https://doi.org/10.1111/gcb.16804, 2023.

Breiman, L.: Random forests, Mach. Learn., 45, 5–32, https://doi.org/10.1023/A:1010933404324, 2001.

Cambardella, C. A. and Elliott, E. T.: Particulate soil organic-matter changes across a grassland cultivation sequence, Soil Sci. Soc. Am. J., 56, 777–783, https://doi.org/10.2136/sssaj1992.03615995005600030017x, 1992.

Cécillon, L.: A dual response, Nat. Geosci., 14, 262–263, https://doi.org/10.1038/s41561-021-00749-6, 2021.

Cécillon, L., Baudin, F., Chenu, C., Houot, S., Jolivet, R., Kätterer, T., Lutfalla, S., Macdonald, A., van Oort, F., Plante, A. F., Savignac, F., Soucémarianadin, L. N., and Barré, P.: A model based on Rock-Eval thermal analysis to quantify the size of the centennially persistent organic carbon pool in temperate soils, Biogeosciences, 15, 2835–2849, https://doi.org/10.5194/bg-15-2835-2018, 2018.

Cécillon, L., Baudin, F., Chenu, C., Christensen, B. T., Franko, U., Houot, S., Kanari, E., Kätterer, T., Merbach, I., van Oort,

F., Poeplau, C., Quezada, J. C., Savignac, F., Soucémarianadin, L. N., and Barré, P.: Partitioning soil organic carbon into its centennially stable and active fractions with machine-learning models based on Rock-Eval® thermal analysis ($PARTY_{SOC}$v2.0 and $PARTY_{SOC}v2.0_{EU}$), Geosci. Model Dev., 14, 3879–3898, https://doi.org/10.5194/gmd-14-3879-2021, 2021.

Chassé, M., Lutfalla, S., Cécillon, L., Baudin, F., Abiven, S., Chenu, C., and Barré, P.: Long-term bare-fallow soil fractions reveal thermo-chemical properties controlling soil organic carbon dynamics, Biogeosciences, 18, 1703–1718, https://doi.org/10.5194/bg-18-1703-2021, 2021.

Chen, S., Arrouays, D., Angers, D. A., Martin, M. P., and Walter, C.: Soil carbon stocks under different land uses and the applicability of the soil carbon saturation concept, Soil Till. Res., 188, 53–58, https://doi.org/10.1016/j.still.2018.11.001, 2019.

Clivot, H., Mouny, J. C., Duparque, A., Dinh, J. L., Denoroy, P., Houot, S., Vertès, F., Trochard, R., Bouthier, A., Sagot, S., and Mary, B.: Modeling soil organic carbon evolution in long-term arable experiments with AMG model, Environ. Modell. Softw., 118, 99–113, https://doi.org/10.1016/j.envsoft.2019.04.004, 2019.

Cotrufo, M. F., Soong, J. L., Horton, A. J., Campbell, E. E., Haddix, M. L., Wall, D. H., and Parton, W. J.: Formation of soil organic matter via biochemical and physical pathways of litter mass loss, Nat. Geosci., 8, 776–779, https://doi.org/10.1038/ngeo2520, 2015.

Cotrufo, M. F., Ranalli, M. G., Haddix, M. L., Six, J., and Lugato, E.: Soil carbon storage informed by particulate and mineral-associated organic matter, Nat. Geosci., 12, 989–994, https://doi.org/10.1038/s41561-019-0484-6, 2019.

Cotrufo, M. F., Lavallee, J. M., Six, J., and Lugato, E.: The robust concept of mineral-associated organic matter saturation: A letter to Begill et al., 2023, Global Change Biol., 29, 5986–5987, https://doi.org/10.1111/gcb.16921, 2023.

Delahaie, A., Baudin, F., Cécillon, L., Savignac, F., and Barré, P.: Rock-Eval® thermal analysis results of the first RMQS campaign topsoil samples, Recherche Data Gouv [data set], https://doi.org/10.57745/KVUTRB, 2024.

Delahaie, A. A., Barré, P., Baudin, F., Arrouays, D., Bispo, A., Boulonne, L., Chenu, C., Jolivet, C., Martin, M. P., Ratié, C., Saby, N. P. A., Savignac, F., and Cécillon, L.: Elemental stoichiometry and Rock-Eval® thermal stability of organic matter in French topsoils, SOIL, 9, 209–229, https://doi.org/10.5194/soil-9-209-2023, 2023.

Disnar, J. R., Guillet, B., Kéravis, D., Di-Giovanni, C., and Sebag, D.: Soil organic matter (SOM) characterization by Rock-Eval pyrolysis: scope and limitations, Org. Geochem., 34, 327–343, https://doi.org/10.1016/S0146-6380(02)00239-5, 2003.

Edlinger, A., Garland, G., Banerjee, S., Degrune, F., García-Palacios, P., Herzog, C., Pescador, D. S., Romdhane, S., Ryo, M., Saghaï, A., Hallin, S., Maestre, F. T., Philippot, L., Rillig, M. C., and van Der Heijden, M. G.: The impact of agricultural management on soil aggregation and carbon storage is regulated by climatic thresholds across a 3000 km European gradient, Global Change Biol., 29, 3177–3192, https://doi.org/10.1111/gcb.16677, 2023.

Eggleston, H. S., Buendia, L., Miwa, K., Ngara, T., and Tanabe, K.: 2006 IPCC guidelines for national greenhouse gas inventories, Institute for Global Environmental Strategies (IGES), ISBN 4-88788-032-4, 2006.

Fox, J. and Weisberg, S.: An R Companion to Applied Regression, 3rd edn., Sage, Thousand Oaks CA, https://www.john-fox.ca/Companion/ (last access: 3 October 2024), 2019.

Georgiou, K., Jackson, R. B., Vindušková, O., Abramoff, R. Z., Ahlström, A., Feng, W., Harden, J. W., Pellegrini, A. F. A., Polley, H. W., Soong, J. L., Riley, W. J., and Torn, M. S.: Global stocks and capacity of mineral-associated soil organic carbon, Nat. Commun., 13, 3797, https://doi.org/10.1038/s41467-022-31540-9, 2022.

Gogé, F., Joffre, R., Jolivet, C., Ross, I., and Ranjard, L.: Optimization criteria in sample selection step of local regression for quantitative analysis of large soil NIRS database, Chemometr. Intell. Lab., 110, 168–176, https://doi.org/10.1016/j.chemolab.2011.11.003, 2012.

Hansen, P. S., Even, R., King, A. E., Lavallee, J., Schipanski, M., and Cotrufo, M. F.: Distinct, direct and climate-mediated environmental controls on global particulate and mineral-associated organic carbon storage, Global Change Biol., 30, e17080, https://doi.org/10.1111/gcb.17080, 2024.

Janzen, H. H.: The soil carbon dilemma: shall we hoard it or use it?, Soil Biol. Biochem., 38, 419–424, https://doi.org/10.1016/j.soilbio.2005.10.008, 2006.

Jolivet, C., Boulonne, L., and Ratié, C.: Manuel du Réseau de Mesures de la Qualité des Sols, édition 2006, Unité InfoSol, INRA Orléans, France, 190 pp., ISBN 2-73-80-1235-3, 2006.

Jolivet, C., Almeida Falcon, J.-L., Berché, P., Boulonne, L., Fontaine, M., Gouny, L., Lehmann, S., Maître, B., Ratié, C., Schellennberger, E., and Soler-Dominguez, N.: French Soil Quality Monitoring Network Manual RMQS2: second metropolitan campaign 2016–2027, ISBN 2-7380-1451-8, https://doi.org/10.17180/KC64-NY88, 2022.

Kanari, E., Cécillon, L., Baudin, F., Clivot, H., Ferchaud, F., Houot, S., Levavasseur, F., Mary, B., Soucémarianadin, L., Chenu, C., and Barré, P.: A robust initialization method for accurate soil organic carbon simulations, Biogeosciences, 19, 375–387, https://doi.org/10.5194/bg-19-375-2022, 2022.

Kassambara, A.: ggpubr: "ggplot2" Based Publication Ready Plots. R package version 0.6.0, https://rpkgs.datanovia.com/ggpubr/ (last access: 8 February 2023), 2023a.

Kassambara, A.: rstatix: Pipe-Friendly Framework for Basic Statistical Tests. R package version 0.7.2, https://rpkgs.datanovia.com/rstatix/ (last access: 8 February 2023), 2023b.

Kassambara, A. and Mundt, F.: Factoextra: Extract and Visualize the Results of Multivariate Data Analyses. R Package Version 1.0.7, https://CRAN.R-project.org/package=factoextra (last access: 8 February 2023), 2020.

King, A. E., Amsili, J. P., Córdova, S. C., Culman, S., Fonte, S. J., Kotcon, J., Liebig, M., Masters, M. D., McVay, K., Olk, D. C., Schipanski, M., Schneider, S. K., Stewart, C. E., and Cotrufo, M. F.: A soil matrix capacity index to predict mineral-associated but not particulate organic carbon across a range of climate and soil pH, Biogeochemistry, 165, 1–14, https://doi.org/10.1007/s10533-023-01066-3, 2023.

Kleber, M., Eusterhues, K., Keiluweit, M., Mikutta, C., Mikutta, R., and Nico, P. S.: Mineral–organic associations: formation, properties, and relevance in soil environments, Adv. Agron., 130, 1–140, https://doi.org/10.1016/bs.agron.2014.10.005, 2015.

Kögel-Knabner, I., Guggenberger, G., Kleber, M., Kandeler, E., Kalbitz, K., Scheu, S., Eusterhues, K., and Leinweber, P.: Organo-mineral associations in temperate soils: Integrating biology, mineralogy, and organic matter chemistry, J. Plant Nutr. Soil Sc., 171, 61–82, https://doi.org/10.1002/jpln.200700048, 2008.

Lavallee, J. M., Soong, J. L., and Cotrufo, M. F.: Conceptualizing soil organic matter into particulate and mineral-associated forms to address global change in the 21st century, Global Change Biol., 26, 261–273, https://doi.org/10.1002/jpln.200700048, 2020.

Le Noë, J., Manzoni, S., Abramoff, R., Bölscher, T., Bruni, E., Cardinael, R., Ciais, P., Chenu, C., Clivot, H., Derrien, D., Ferchaud, F., Garnier, P., Goll, D., Lashermes, G., Martin, M., Rasse, D., Rees, F., Sainte-Marie, J., Salmon, E., Schiedung, M., Schimel, J., Wieder, W., Abiven, S., Barré, P., Cécillon, L., and Guenet, B.: Soil organic carbon models need independent time-series validation for reliable prediction, Communications Earth and Environment, 4, 158, https://doi.org/10.1038/s43247-023-00830-5, 2023.

Louppe, G.: Understanding random forests: From theory to practice, arXiv [preprint], https://doi.org/10.48550/arXiv.1407.7502, 2014.

Louppe, G., Wehenkel, L., Sutera, A., and Geurts, P.: Understanding variable importances in forests of randomized trees, Adv. Neur. In., 26, ISBN 9781632660244, 2013.

Lugato, E., Lavallee, J. M., Haddix, M. L., Panagos, P., and Cotrufo, M. F.: Different climate sensitivity of particulate and mineral-associated soil organic matter, Nat. Geosci., 14, 295–300, https://doi.org/10.1038/s41561-021-00744-x, 2021.

Luo, Y., Ahlström, A., Allison, S. D., Batjes, N. H., Brovkin, V., Carvalhais, N., Chappell, A., Ciais, P., Davidson, E. A., Finzi, A., Georgiou, K., Guenet, B., Hararuk, O., Harden, J. W., He, Y., Hopkins, F., Jiang, L., Koven, C., Jackson, R. B., Jones, C. D., Lara, M. J., Liang, J., McGuire, A. D., Parton, W., Peng, C., Randerson, J. T., Salazar, A., Sierra, C. A., Smith, M. J., Tian, H., Todd-Brown, K. E. O., Torn, M., Van Groenigen, K. J., Wang, Y. P., West, T. O., Wei, Y., Wieder, W. R., Xia, J., Xu, X., Xu, X., and Zhou, T.: Toward more realistic projections of soil carbon dynamics by Earth system models, Global Biogeochem. Cy., 30, 40–56, https://doi.org/10.1002/2015GB005239, 2016.

Mathieu, J. A., Hatté, C., Balesdent, J., and Parent, É.: Deep soil carbon dynamics are driven more by soil type than by climate: a worldwide meta-analysis of radiocarbon profiles, Global Change Biol., 21, 4278–4292, https://doi.org/10.1111/gcb.13012, 2015.

Pacini, L., Adatte, T., Barré, P., Boussafir, M., Bouton, N., Cécillon, L., Lamoureux-Var, V., Sebag, D., Verrechia, E., Wattripont, A., and Baudin, F.: Reproducibility of Rock-Eval® thermal analysis for soil organic matter characterization, Org. Geochem., 186, 104687, https://doi.org/10.1016/j.orggeochem.2023.104687, 2023.

Pedregosa, F., Varoquaux, G., Gramfort, A., Michel, V., Thirion, B., Grisel, O., Blondel, M., Prettenhofer, P., Weiss, R., Dubourg, V., Vanderplas, J., Passos, A., Cournapeau, D., Brucher, M., Perrot, M., and Duchesnay, É.: Scikit-learn: Machine learning in Python, J. Mach. Learn. Res., 12, 2825–2830, 2011.

Plante, A. F., Fernández, J. M., and Leifeld, J.: Application of thermal analysis techniques in soil science, Geoderma, 153, 1–10, https://doi.org/10.1016/j.geoderma.2009.08.016, 2009.

Poeplau, C. and Don, A.: Sensitivity of soil organic carbon stocks and fractions to different land-use changes across Europe, Geoderma, 192, 189–201, https://doi.org/10.1016/j.geoderma.2012.08.003, 2013.

Poeplau, C., Don, A., Six, J., Kaiser, M., Benbi, D., Chenu, C., Cotrufo, M. F., Derrien, D., Gioacchini, P., Grand, S., Gregorich, E., Griepentrog, M., Gunina, A., Haddix, M., Kuzyakov, Y., Kühnel, A., Macdonald, L. M., Soong, J., Trigalet, S., Vermeire, M.-L., Rovira, P., van Wesemael, B., Wiesmeier, M., Yeasmin, S., Yevdokimov, I., and Nieder, R.: Isolating organic carbon fractions with varying turnover rates in temperate agricultural soils–A comprehensive method comparison, Soil Biol. Biochem., 125, 10–26, https://doi.org/10.1016/j.soilbio.2018.06.025, 2018.

Rowley, M. C., Grand, S., and Verrecchia, É. P.: Calcium-mediated stabilisation of soil organic carbon, Biogeochemistry, 137, 27–49, https://doi.org/10.1007/s10533-017-0410-1, 2018.

Rowley, M. C., Grand, S., Spangenberg, J. E., and Verrecchia, E. P.: Evidence linking calcium to increased organo-mineral association in soils, Biogeochemistry, 153, 223–241, https://doi.org/10.1007/s10533-021-00779-7, 2021.

Rumpel, C., Amiraslani, F., Chenu, C., Garcia Cardenas, M., Kaonga, M., Koutika, L. S., Ladha, J., Madari, B., Shirato, Y., Smith, P., Soudi, B., Soussana, J.-F., Whitehead, D., and Wollenberg, E.: The 4p1000 initiative: Opportunities, limitations and challenges for implementing soil organic carbon sequestration as a sustainable development strategy, Ambio, 49, 350–360, https://doi.org/10.1007/s13280-019-01165-2, 2020.

Saby, N., Bertouy, B., Boulonne, L., Bispo, A., Ratié, C., and Jolivet, C.: Statistiques sommaires issues du RMQS sur les données agronomiques et en éléments traces des sols français de 0 à 50 cm, V5, Portail Data INRAE [data set], https://doi.org/10.15454/BNCXYB, 2019.

Saenger, A., Cécillon, L., Sebag, D., and Brun, J. J.: Soil organic carbon quantity, chemistry and thermal stability in a mountainous landscape: A Rock–Eval pyrolysis survey, Org. Geochem., 54, 101–114, https://doi.org/10.1016/j.orggeochem.2012.10.008, 2013.

Sanderman, J., Baldock, J. A., Dangal, S. R. S. Ludwig, S., Potter, S., Rivard, C., and Savage, K.: Soil organic carbon fractions in the Great Plains of the United States: an application of mid-infrared spectroscopy, Biogeochemistry, 156, 97–114, https://doi.org/10.1007/s10533-021-00755-1, 2021.

Schmidt, M. W., Torn, M. S., Abiven, S., Dittmar, T., Guggenberger, G., Janssens, I. A., Kleber, M., Kögel-Knabner, I., Lehmann, J., Manning, D. A. C., Nannipieri, P., Rasse, D. P., Weiner, S., and Trumbore, S. E.: Persistence of soil organic matter as an ecosystem property, Nature, 478, 49–56, https://doi.org/10.1038/nature10386, 2011.

Schrumpf, M., Kaiser, K., Guggenberger, G., Persson, T., Kögel-Knabner, I., and Schulze, E.-D.: Storage and stability of organic carbon in soils as related to depth, occlusion within aggregates, and attachment to minerals, Biogeosciences, 10, 1675–1691, https://doi.org/10.5194/bg-10-1675-2013, 2013.

Sebag, D., Verrecchia, E. P., Cécillon, L., Adatte, T., Albrecht, R., Aubert, M., Bureau, F., Cailleau, G., Copard, Y., Decaens, T., Disnar, J.-R., Hetényi, M., Nyilas, T., and Trombino, L.: Dynamics of soil organic matter based on new Rock-Eval indices, Geoderma, 284, 185–203, https://doi.org/10.1016/j.geoderma.2016.08.025, 2016.

Soetaert, K.: plot3D: Plotting Multi-Dimensional Data. (Version 1.4), https://cran.rproject.org/web/packages/plot3D/plot3D.pdf (last access: 8 February 2023), 2021.

Soucémarianadin, L., Cécillon, L., Chenu, C., Baudin, F., Nicolas, M., Girardin, C., and Barré, P.: Is Rock-Eval 6 thermal analysis a good indicator of soil organic carbon lability? – A method-comparison study in forest soils, Soil Biol. Biochem., 117, 108–116, https://doi.org/10.1016/j.soilbio.2017.10.025, 2018.

Soucémarianadin, L., Cécillon, L., Chenu, C., Baudin, F., Nicolas, M., Girardin, C., Delahaie, A. A., and Barré, P.: Heterogeneity of the chemical composition and thermal stability of particulate organic matter in French forest soils, Geoderma, 342, 65–74, https://doi.org/10.1016/j.geoderma.2019.02.008, 2019.

Stojanova, M. and Delahaie, A.: SOC fractions drivers, Zenodo [code], https://doi.org/10.5281/zenodo.10551240, 2024.

Vinci Technologies (Nanterre, France): Geoworks V1.6R2, https://www.vinci-technologies.com/rocks-and-fluids/geology/organic-geochemistry/geoworks-geochemical-software/113335/ (last access: 12 June 2023), 2021.

Virtanen, P., Gommers, R., Oliphant, T. E., Haberland, M., Reddy, T., Cournapeau, D., Burovski, E., Peterson, P., Weckesser, W., Bright, J., van der Walt, S. J., Brett, M., Wilson, J., Millman, K. J., Mayorov, N., Nelson, A. R. J., Jones, E., Kern, R., Larson, E., Carey, C. J., Polat, I., Feng, Y., Moore, E. W., Vanderplas, J., Laxalde, D., Perktold, J., Cimrman, R., Henriksen, I., Quintero, E. A., Harris, C. R., Archibald, A. M., Ribeiro, A. H., Pedragosa, F., and Van Mulbregt, P.: SciPy 1.0: fundamental algorithms for scientific computing in Python, Nat. Methods, 17, 261–272, https://doi.org/10.1038/s41592-019-0686-2, 2020.

Viscarra Rossel, R. A., Lee, J., Behrens, T., Luo, Z., Baldock, J., and Richards, A.: Continental-scale soil carbon composition and vulnerability modulated by regional environmental controls, Nat. Geosci., 12, 547–552, https://doi.org/10.1038/s41561-019-0373-z, 2019.

von Lützow, M., Kögel-Knabner, I., Ekschmitt, K., Flessa, H., Guggenberger, G., Matzner, E., and Marschner, B.: SOM fractionation methods: relevance to functional pools and to stabilization mechanisms, Soil Biol. Biochem., 39, 2183–2207, https://doi.org/10.1016/j.soilbio.2007.03.007, 2007.

von Lützow, M. V., Kögel-Knabner, I., Ekschmitt, K., Matzner, E., Guggenberger, G., Marschner, B., and Flessa, H.: Stabilization of organic matter in temperate soils: mechanisms and their relevance under different soil conditions – a review, Eur. J. Soil Sci., 57, 426–445, https://doi.org/10.1111/j.1365-2389.2006.00809.x, 2006.

Wei, T. and Simko, V.: R package "corrplot": Visualization of a Correlation Matrix (Version 0.92), https://github.com/taiyun/corrplot (last access: 8 February 2023), 2021.

Wickham, H.: ggplot2: Elegant Graphics for Data Analysis, Springer-Verlag, New York, ISBN 978-3-319-24277-4, 2016.

Zimmermann, M., Leifeld, J., Schmidt, M. W. I., Smith, P., and Fuhrer, J.: Measured soil organic matter fractions can be related to pools in the RothC model, Eur. J. Soil Sci., 58, 658–667, https://doi.org/10.1111/j.1365-2389.2006.00855.x, 2007.